The EMBO Journal (2011) 30, 364–378 | © 2011 European Molecular Biology Organization | Some Rights Reserved 0261-4189/11
www.embojournal.org

THE EMBO JOURNAL

EMBO open

A positively charged channel within the Smc1/Smc3 hinge required for sister chromatid cohesion

Alexander Kurze[1], Katharine A Michie[2], Sarah E Dixon[1], Ajay Mishra[1], Takehiko Itoh[3], Syma Khalid[4], Lana Strmecki[1], Katsuhiko Shirahige[5], Christian H Haering[6], Jan Löwe[2] and Kim Nasmyth[1,*]

[1]Department of Biochemistry, University of Oxford, Oxford, UK, [2]MRC Laboratory of Molecular Biology, Cambridge, UK, [3]Laboratory of *In Silico* Functional Genomics, Graduate School of Bioscience, Tokyo Institute of Technology, Yokohama, Japan, [4]School of Chemistry, University of Southampton, Southampton, UK, [5]Laboratory of Genome Structure and Function, Research Center for Epigenetic Disease, Institute of Molecular and Cellular Biosciences, The University of Tokyo, Tokyo, Japan and [6]European Molecular Biology Laboratory, Heidelberg, Germany

Cohesin's structural maintenance of chromosome 1 (Smc1) and Smc3 are rod-shaped proteins with 50-nm long intramolecular coiled-coil arms with a heterodimerization domain at one end and an ABC-like nucleotide-binding domain (NBD) at the other. Heterodimerization creates V-shaped molecules with a hinge at their centre. Interconnection of NBDs by Scc1 creates a tripartite ring within which, it is proposed, sister DNAs are entrapped. To investigate whether cohesin's hinge functions as a possible DNA entry gate, we solved the crystal structure of the hinge from *Mus musculus*, which like its bacterial counterpart is characterized by a pseudo symmetric heterodimeric torus containing a small channel that is positively charged. Mutations in yeast Smc1 and Smc3 that together neutralize the channel's charge have little effect on dimerization or association with chromosomes, but are nevertheless lethal. Our finding that neutralization reduces acetylation of Smc3, which normally occurs during replication and is essential for cohesion, suggests that the positively charged channel is involved in a major conformational change during S phase.

The EMBO Journal (2011) **30,** 364–378. doi:10.1038/emboj.2010.315; Published online 7 December 2010
Subject Categories: cell cycle; structural biology
Keywords: cohesin; hinge; Smc1; Smc3; structure

*Corresponding author. Department of Biochemistry, University of Oxford, South Parks Road, Oxford OX1 3QU, UK. Tel.: +44 186 561 3229; Fax: +44 186 561 3341; E-mail: kim.nasmyth@bioch.ox.ac.uk

Received: 14 August 2010; accepted: 11 November 2010; published online: 7 December 2010

Introduction

In eukaryotic cells, sister chromatids are held together from their genesis during DNA replication until their disjunction at the metaphase-to-anaphase transition by a complex called cohesin composed of structural maintenance of chromosomes (SMC) proteins Smc1 and Smc3, a kleisin subunit Scc1 (Rad21), Scc3 (SA1/SA2) and a less tightly associated protein called Pds5 (Nasmyth and Haering, 2005). Cohesin's Smc1 and Smc3 subunits fold back on themselves to form 50-nm long rod-shaped intra-molecular anti-parallel coiled coils, with globular 'hinge' domains at one end and an ABC-like nucleotide-binding domain (NBD) at the other end. Heterotypic interactions between Smc1 and Smc3 hinges create stable V-shaped Smc1/Smc3 heterodimers (Melby *et al*, 1998; Haering *et al*, 2002; Hirano and Hirano, 2002), which are converted to closed rings by inter-connection of their NBDs by cohesin's Scc1 α-kleisin subunit, whose N- and C-terminal domains bind to Smc3 and Smc1, respectively (Nasmyth and Haering, 2005). In addition to this kleisin-mediated inter-connection, Smc1 and Smc3 NBDs can directly engage in the presence of ATP. Only when engaged in this manner, can ATP molecules sandwiched between Smc1 and Smc3 NBDs be hydrolysed (Arumugam *et al*, 2006), a process that is essential for cohesin's association with chromosomes (Arumugam *et al*, 2003; Weitzer *et al*, 2003).

Cohesin's association with chromosomes requires the action of a separate Scc2/Scc4 complex (Ciosk *et al*, 2000), whereas its ability to connect sister DNAs during S phase requires acetylation of Smc3's NBD by the acetyltransferase Eco1 (Skibbens *et al*, 1999; Toth *et al*, 1999; Ivanov *et al*, 2002; Ben-Shahar *et al*, 2008; Unal *et al*, 2008; Rowland *et al*, 2009). The dissolution of sister chromatid cohesion, which takes place only when all chromosomes have bi-oriented on the mitotic spindle, is triggered by cleavage of cohesin's Scc1 α-kleisin subunit by the thiol protease separase (Uhlmann *et al*, 1999, 2000; Waizenegger *et al*, 2000; Hauf *et al*, 2001). In yeast, most cohesin rings are destroyed by separase (Uhlmann *et al*, 1999, 2000) and cohesin's re-association with chromosomes depends on re-synthesis of Scc1 shortly before S phase (Michaelis *et al*, 1997).

It has been suggested that cohesin associates stably with chromatin by entrapping DNAs inside its ring (Haering *et al*, 2002; Gruber *et al*, 2003). As predicted by this hypothesis, circular sister minichromosomes remain trapped inside rings whose three interfaces have been chemically cross-linked, even after denaturation (Haering *et al*, 2008). This also implies that cohesion does not involve hitherto uncharacterized interactions between cohesin rings (Zhang *et al*, 2008).

DNA entrapment by cohesin rings presumably entails transient ring opening, that is, the ring must have an entry gate. The finding that cohesin remains functional even after (co-translational) fusion of Smc3 to Scc1 or Scc1 to Smc1 suggests that the entry gate may be situated at the hinge dimerization interface (Gruber *et al*, 2006). Consistent with this notion is the observation that rapamycin-induced connection of Smc1 and Smc3 hinge domains containing FKBP12 and Frb dimerization domains, respectively, blocks establishment but not maintenance of sister chromatid cohesion (Gruber *et al*, 2006).

To investigate the notion that the Smc1/Smc3 hinge domain has functions besides merely holding Smc1 and Smc3 together, we solved the mouse Smc1/Smc3 hinge crystal structure, which closely resembles the homodimeric bacterial *Thermotoga maritima* SMC hinge (Haering *et al*, 2002). In both cases, shallow U-shaped hinge monomers interact to form a pseudo twofold symmetric torus with a small channel in the middle. Remarkably, the channel is positively charged, a feature that, according to modelling, is conserved in SMC hinges from widely different eukaryotic and prokaryotic organisms. We describe a set of amino-acid substitutions in budding yeast Smc1 and Smc3 that, when combined, largely eliminate the channel's positive charge without greatly changing the equilibrium association constant, but reduce the rate of hinge dissociation (K_{off}) *in vitro*. Although the neutralizing mutations permit formation of cohesin rings *in vivo* whose stable association with the genome resembles wild-type cohesin, they drastically reduce Smc3 acetylation and establishment of cohesion during S phase. These data are inconsistent with the notion that Smc1/Smc3 hinges merely act as dimerization domains. They suggest that hinges participate in a major conformational change during S phase, possibly hinge opening, linked to acetylation of Smc3's NBD.

Results

The structure of the mouse Smc1/Smc3 hinge heterodimer resembles the bacterial SMC hinge homodimer

The *Mus musculus* Smc1/Smc3 hinge heterodimer complex was obtained by co-overexpression of Smc1 residues 471–685 followed by a C-terminal 6xHis tag and Smc3 residues 484–696 in *Escherichia coli*. We crystallized the Smc1/Smc3 complex and solved its structure using single-wavelength anomalous diffraction data and molecular replacement with the bacterial *T. maritima* SMC hinge domain structure (Figure 1, Supplementary Tables 1 and 2). Because Smc1 and Smc3 from *M. musculus* are more similar to each other in primary amino-acid sequence than they are to the *T. maritima* SMC hinge domain, multi-wavelength anomalous diffraction experiments using SeMet-substituted derivatives of both Smc1 (2-ordered Met) and Smc3 (6-ordered Met) in complex were required to assign each monomer within the heterodimer. The resulting structure was refined to 2.7 Å (Supplementary Table 1). The crystals contained one heterodimer of the Smc1/Smc3 complex, ordered between residues 499 and 675 for Smc1 (chain A), and residues 492 and 670, and 674 and 685 for Smc3 (chain B).

The protein fold of the *M. musculus* Smc1/Smc3 heterodimer resembles the previously published structure of the hinge domain of the SMC homodimer from *T. maritima* (PDB 1GXL; Haering *et al*, 2002; Figure 1A). Both N- and C termini of Smc1 and Smc3 hinge domains are present on the same face of the dimer (Figure 1B) and their orientation is consistent with the formation of intra-molecular coiled coils within the 'arms' of the Smc1/Smc3 heterodimers (Haering *et al*, 2002). Surface representations of the *M. musculus* hinge domain suggest that there is a small channel running through the centre of the dimerization interface (Figure 1C), as also found in the *T. maritima* structure. By taking atomic radii into account, the smallest aperture within the channel was determined to be ~5 Å in diameter, and neither dsDNA nor protein would be able to pass through the channel in the conformation crystallized (Figure 1C, centre).

Eukaryotic and prokaryotic SMC hinge channels are positively charged

Calculation of the surface electrostatics of the *M. musculus* Smc1/Smc3 hinge domains reveals that its central channel is highly positively charged, owing to it being lined with many arginines and lysines (Figures 1C and 2B). *In silico* protein modelling of a large number of prokaryotic SMC complexes (modelled on the *T. maritima* SMC complex hinge structure) and eukaryotic Smc1/Smc3 hinge domains (modelled on the *M. musculus* Smc1/Smc3 hinge structure presented here) suggests that the positive charge is a highly conserved feature of the central channel (Figure 2A and Supplementary Figures 1 and 2). Surprisingly, a recently published crystal structure of a conformationally open condensin hinge (mSmc2/mSmc4) revealed rather few positive charges within its inner surface (Griese *et al*, 2010). The protein used for crystallization, however, lacks a C-terminal β-strand of Smc4 and, as a result, two lysine residues are missing that would point towards the inner surface of the channel. Modelling revealed that an intact and fully closed condensin hinge would also contain a positively charged hinge channel (data not shown). Interestingly, two groups have recently solved the crystal structure of the *E. coli* MukB homodimeric hinge, which lacks the channel and as a consequence few positive charges are positioned between the dimerization interface (Ku *et al*, 2010; Li *et al*, 2010).

The positively charged residues in the hinge channel are essential for cohesin's function

To investigate the physiological importance of the channel's positive charge, we introduced into Smc1 and Smc3 from *Saccharomyces cerevisiae* five amino-acid substitutions that together neutralize the charge (Figure 2B and Supplementary Figure 4) without obviously altering the dimerization interface itself. K554 and K661 were mutated to aspartic acid within the Smc1 half hinge (*smc1DD*), while K668, R665 and R669 were mutated to alanine within the Smc3 half hinge (*smc3AAA*). *In silico* modelling shows that only by combining Smc1DD with Smc3AAA is the channel's positive charge largely eliminated (Supplementary Figure 4). Tetrad analysis of spores from a heterozygous *SMC1/smc1*Δ diploid strain revealed that a single ectopic copy of *smc1DD-myc9* fully rescues *smc1*Δ cells. Similarly, a single ectopic copy of *smc3AAA-HA3* fully rescues *smc3*Δ cells (Supplementary Figure 5A). In contrast, analysis of tetrads from double heterozygous *SMC3/smc3*Δ *SMC1/smc1*Δ diploid strains revealed that (unlike their wild-type counterparts) ectopic copies of *smc3AAA-HA3* and *smc1DD-myc9* together fail

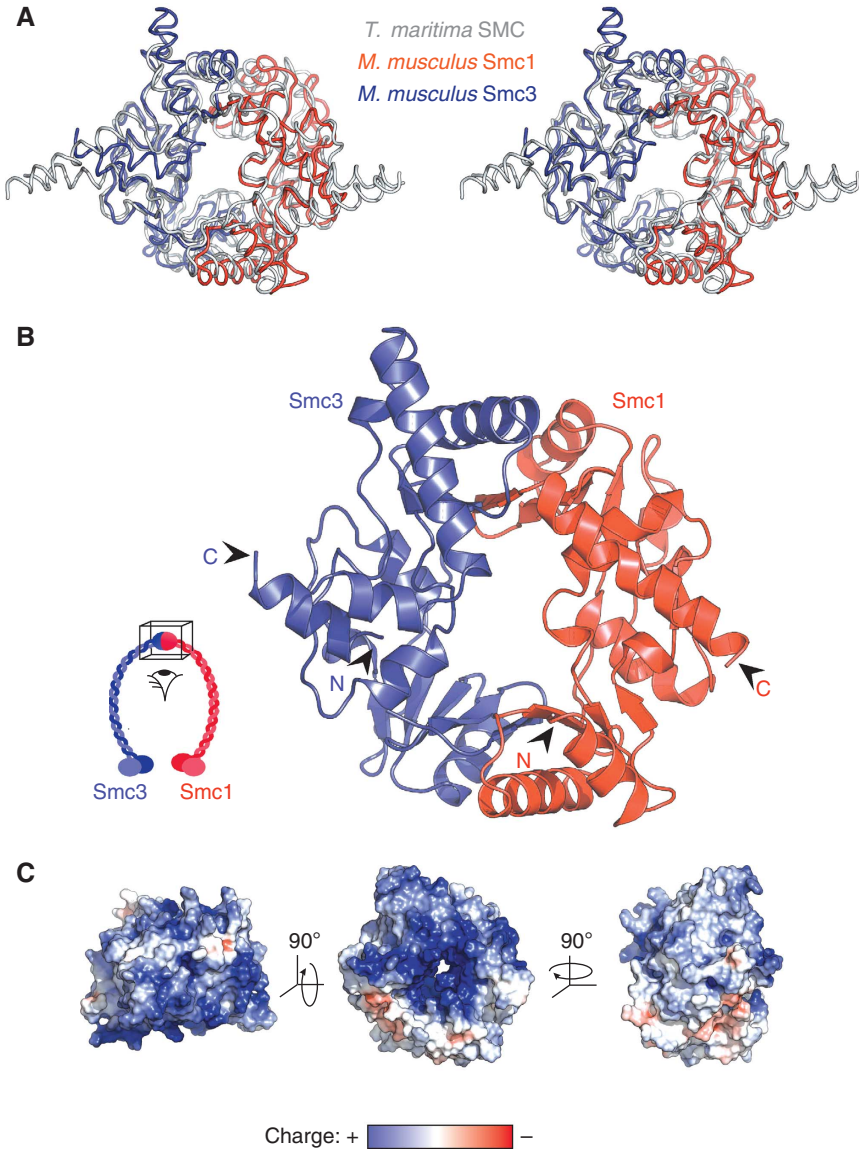

Figure 1 The *M. musculus* heterodimeric Smc1/Smc3 hinge domain is structurally similar to the bacterial *T. maritima* SMC hinge homodimer. (**A**) Stereo overlay in ribbon depiction of the *M. musculus* Smc1 (red) and Smc3 (blue) hinge domain structure with the bacterial *T. maritima* SMC hinge domain (grey). (**B**) Cartoon representation of the *M. musculus* Smc1/Smc3 hinge domain. (**C**) Surface depictions of the *M. musculus* Smc1/Smc3 hinge domains with electrostatic potentials mapped onto the surface, showing the central channel through the molecule and the highly charged nature of the channel. Images shown are 90° rotations about the *x* and *y* axis.

to complement *smc3*Δ *smc1*Δ double deletion mutants (Supplementary Figure 5A).

To investigate the effect on sister chromatid cohesion, we used a strain in which the *URA3* locus is marked by the binding of Tet repressor-GFP to multiple tandem Tet operators (Michaelis *et al*, 1997). Cells expressing the temperature-sensitive *smc3-42* allele together with either wild-type or Smc1DD/Smc3AAA proteins were first arrested in metaphase by depleting Cdc20 (for 1 h at 25°C) and then shifted to 35°C for 3 h to inactivate *smc3-42*. Sister *URA3* loci marked by GFP split in only 10% of cells expressing wild-type Smc1/Smc3, but in 70% of cells expressing Smc1DD/Smc3AAA (Figure 6C). We conclude that Smc1DD/Smc3AAA proteins are unable to generate sister chromatid cohesion.

To test the effect of charge neutralization on cohesin complex formation *in vivo*, we created yeast strains that express Smc1-myc9 or Smc1DD-myc9, Scc1-PK9 (9xGKPIPNPLLGLDST) and Pds5-PK6 instead of wild-type Smc1, Scc1 and Pds5 proteins, as well as Smc3-HA3 or Smc3AAA-HA3 (ectopic copy) together with endogenous Smc3. Western blotting revealed that immunoprecipitates of Smc3-HA3 or Smc3AAA-HA3 contain similar amounts of Smc1-myc9 or Smc1DD-myc9, Scc1-PK9 (Supplementary Figure 5B) and Pds5-PK6 proteins (Supplementary Figure 5C), suggesting that charge neutralization has little or no effect on cohesin complex formation.

Charge-neutralized hinges form stable dimers

To address whether the neutralizing mutations weaken Smc1/Smc3 hinge dimerization, we used both theoretical and empirical approaches. We first compared the conformational stability of wild-type and mutant hinges by molecular dynamic (MD) simulations and found little difference on the timescale evaluated (Supplementary Figure 6). We next used size-exclusion chromatography to compare the dimerization

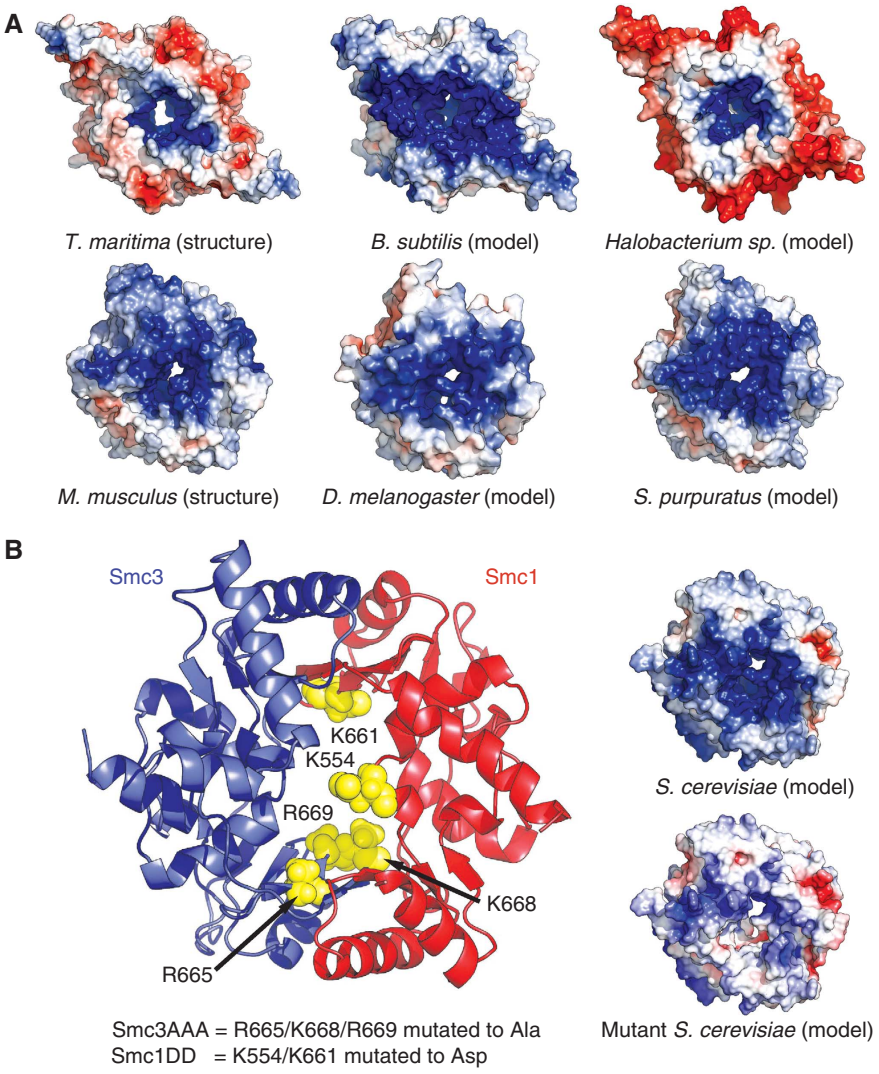

Figure 2 The positively charged central channel is highly conserved in both prokaryotes and eukaryotes. (**A**) Top row of structures shows the electrostatic potentials mapped onto the surfaces of the SMC homodimer hinge domains of *T. maritima* (from X-ray structure), *B. subtilis* and a *Halobacterium* species (both from *in silico* models), revealing a conserved and highly positively charged channel. The bottom row of structures reveals the same highly conserved positive charges within the channels of the *M. musculus* Smc1/Smc3 hinge domain (from X-ray structure), and *Drosophila melanogaster* and *Strongylocentrotus purpuratus* (from *in silico* models). (**B**) The wild-type residues affected by the five mutations (K554D, K661D in Smc1 (Smc1DD); R665A, K668A, R669A in Smc3 (Smc3AAA)) shown in yellow are mapped onto a cartoon depiction of the model of the *S. cerevisiae* Smc1/Smc3 hinge domain complex. The structures showing electrostatic potentials on the right reveal the highly positively charged channel in the wild-type protein (top), and the large reduction in charge within the channel for the mutant protein (bottom).

properties of purified mutant and wild-type hinges *in vitro*. Both monomeric wild-type and mutant Smc hinge proteins elute as single peaks, at approximately 13–14 ml, during analytical size-exclusion chromatography (Figure 3A), which suggests that the neutralizing mutations do not adversely affect folding. In contrast, 1:1 molar ratio mixtures of wild-type Smc1 and Smc3 hinge proteins or Smc1DD and Smc3AAA hinge proteins elute as single peaks shifted to 12 ml (Figure 3A). According to this criterion, the channel-neutralizing mutations have little, if any, adverse effect on dimerization. This was confirmed by isothermal titration calorimetry (ITC), which showed that the dissociation constants (K_d) of wild-type (Smc1/Smc3) and mutant (Smc1DD/Smc3AAA) hinges are 22 and 29 nM, respectively (Figure 3B, left and middle panels). ITC did reveal a 4 kcal/mol reduction in the enthalpy of binding, an effect that cannot *per se* be responsible for the lethality of double-mutant hinges, because the same effect was seen when measuring the binding of wild-type Smc1 and mutant Smc3AAA hinges (Figure 3B, right panel)—a combination that is biologically functional. The enthalpy reduction most likely arises from missing electrostatic interactions; indeed, MD simulation revealed a possible salt bridge (between Smc1 D628 and Smc3 K668) that cannot be formed with the Smc3 K668A mutation.

To address whether the mutations affect dimerization in the context of full-length Smc proteins, we created a yeast strain expressing, in addition to endogenous Smc1, Smc3-HA3 and Smc1-myc9 from their own promoters at ectopic sites. Under these conditions, Smc1 and Smc1-myc9 compete for binding to a limited amount of Smc3-HA3, which was immunoprecipitated from cell extracts and proteins analysed by SDS–PAGE and silver staining (Figure 3C, left lane).

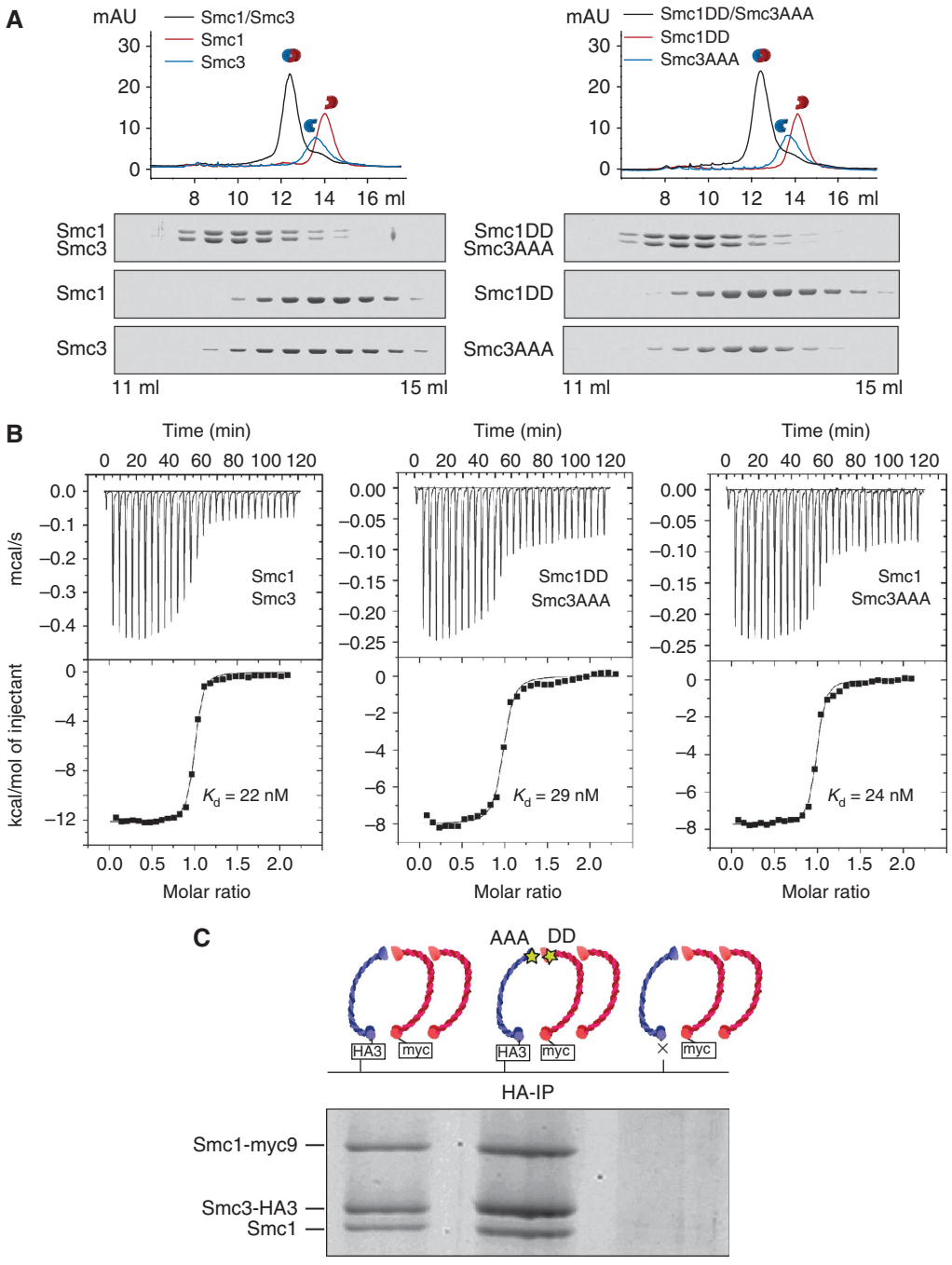

Figure 3 Charge neutralization of the hinge channel does not affect hinge dimerization. (**A**) Smc1DD and Smc3AAA hinge proteins form stable dimers. Smc1 and Smc3 hinges were either injected as monomers or in an equimolar ratio, separated by size-exclusion chromatography, and fractions analysed by SDS–PAGE. After co-incubation for 10 min at 25°C before injection, Smc1 and Smc3 wild-type proteins (left panel) or Smc1DD and Smc3AAA proteins (right panel) form dimers, resulting in earlier elution of the protein fraction compared with monomeric Smc1 and Smc3 proteins. (**B**) Smc1DD and Smc3AAA interact tightly. Smc1/Smc3 association constants were determined by ITC. Changes of heat on successive injections of 10 μl Smc3 (100 μM) in a sample cell containing Smc1 (10 μM) were recorded. The peaks were integrated, normalized to the Smc3 concentration and plotted against the molar ratio of Smc3 to Smc1 protein. Data were fitted using a nonlinear least squares fit to a single-site binding model. The K_d for Smc1 and Smc3 wild-type protein binding is 22 nM (left panel). The K_d for Smc1DD and Smc3AAA hinge domain association is 29 nM (middle panel) and 24 nM for Smc1 wild-type and Smc3AAA (right panel). (**C**) Smc1DD-myc9 competes efficiently with endogenous Smc1 for Smc3AAA-HA3 binding in yeast cell extracts. Control strain (K15426; *SMC1-myc9, SMC3-HA3, SMC1, Δsmc3*; left lane), channel mutant strain (K15423; *smc1DD-myc9, smc3AAA-HA3, SMC1, Δsmc3*; middle lane) and an untagged strain (K11850; right lane) were grown exponentially, cells were lysed and protein immunoprecipitated with anti-HA-beads. Beads were washed, boiled and proteins were analysed by SDS–PAGE and visualized by silver staining.

As expected, similar amounts of Smc1-myc9 and endogenous Smc1 associate with Smc3-HA3. Crucially, a very similar result was obtained with a strain expressing Smc3AAA-HA3 and Smc1DD-myc9 from ectopic sites: Smc3AAA-HA3 co-precipitates similar amounts of mutant and wild-type Smc1 (Figure 3C, middle lane). These results imply that Smc1DD competes efficiently with wild-type Smc1 when binding to Smc3AAA, and that the lethality caused by

channel-neutralizing mutations cannot be caused by impaired Smc1/Smc3 dimerization.

Channel neutralization reduces hinge dissociation

Given that K_{off} divided by K_{on} gives the dissociation constant (K_d), charge neutralization could, in principle, increase (or reduce) both constants without greatly altering the K_d. According to the ring model, an increase in K_{off} could have grave consequences on the maintenance of sister chromatid cohesion, because it would facilitate escape of DNAs from their topological entrapment. To measure K_{off}, we performed a ligand competition assay (Figure 4). Purified monomeric Smc1 and Smc3-FLAG hinges were mixed in an equimolar ratio. After incubation for 10 min, 15 × molar excess of Smc1 competitor protein (Smc1-SNAP) was added and at 15 min intervals, aliquots of this mixture were added to anti-FLAG beads. Control experiments revealed that insignificant amounts of Smc1 hinge are immunoprecipitated by anti-FLAG beads when Smc3-FLAG hinge protein is omitted (Figure 4A). However, owing to required rapid washing steps and its 15 × excess, some Smc1-SNAP bound nonspecifically to anti-FLAG beads. As a consequence, our assay accurately measures the amount of Smc1 associated with Smc3 at different time points, but not the amount of Smc1-SNAP. At the time of competitor addition ($t = 0$), Smc1 and Smc3-FLAG are present in roughly equal proportions in the FLAG immunoprecipitate, indicating efficient binding, but the amount of Smc1 that co-precipitates with Smc3-FLAG gradually declines with time (Figure 4B). Our data suggest that the hinge dimer has a half-life between 15 and 30 min *in vitro*. Similar results were obtained for the biologically functional Smc1/Smc3AAA-FLAG and Smc1DD/Smc3-FLAG heterodimers (Figure 4C and D). Remarkably, this assay revealed that Smc1DD/Smc3AAA-FLAG heterodimers are much more stable than wild-type or single-mutant heterodimers (Figure 4E), with no detectable hinge dissociation even after 90 min. To validate the assay further, we analysed Smc1M665R, which disrupts the 'north' Smc1/Smc3 interface (Mishra *et al*, 2010). This mutation greatly reduces the amount of binding even before competitor addition, as well as the stability of complexes (Figure 4F). Our results suggest that lethality caused by combining Smc1 and Smc3 charge-neutralizing mutations is not due to any intrinsic defect in holding Smc1 and Smc3 together. On the contrary, they raise the possibility that a reduction in K_{off} might instead be responsible.

Hinge channel neutralization has little effect on cohesin's genomic distribution

We used high-throughput sequencing after chromatin immunoprecipitation (ChIP-seq) to investigate the effect on cohesin's association with chromatin. To do this, we generated strains expressing either Smc1-myc9 or Smc1DD-myc9 proteins at physiological levels from ectopic loci together with either Smc3 or Smc3AAA from endogenous loci. Owing to the lethality associated with hinge channel neutralization, both strains also expressed untagged Smc1 from the endogenous locus, ensuring viability of both strains. Myc-tagged proteins were immunoprecipitated from exponentially grown cultures after formaldehyde treatment and DNA fragmentation. After sequencing and mapping reads, visual inspection revealed no major differences between the distributions of wild-type and mutant cohesin complexes (Figure 5A), a conclusion confirmed by a scatter plot of Smc1-myc9 versus Smc1DD-myc9

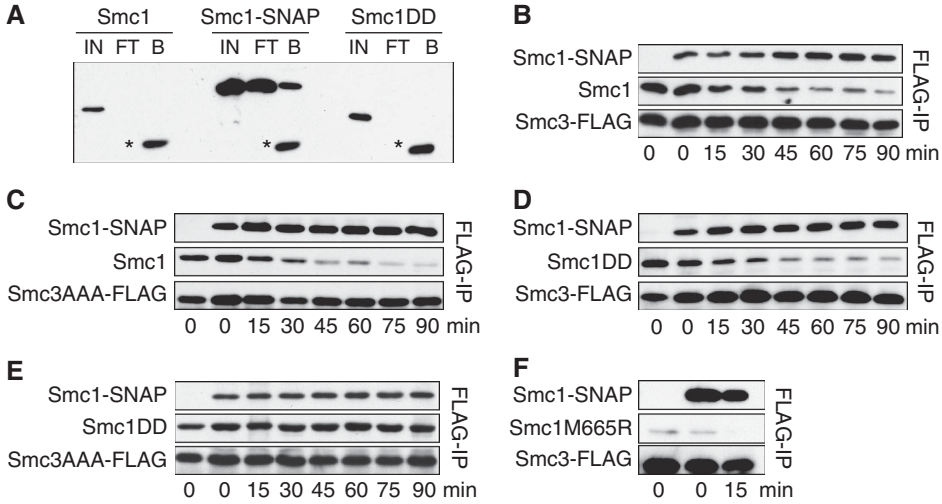

Figure 4 Smc1DD and Smc3AAA form a more stable hinge heterodimer than wild-type Smc1 and Smc3 protein. (**A**) Smc1-SNAP binds anti-FLAG beads unspecifically. A solution of Smc1 (50 nM), Smc1-SNAP (750 nM) or Smc1DD (50 nM) proteins was added to BSA-blocked anti-FLAG beads. Beads were incubated for 10 min at 16°C and washed quickly three times. Samples were boiled and run on a 10% SDS–PAGE, transferred by western blotting, and anti-HIS antibody was used to detect Smc proteins. Asterisks indicate the heavy chain of IgG from bead-coupled anti-FLAG antibodies. (**B**) Smc1 binds to Smc3 with a half time of ~30 min. Smc1 and Smc3-FLAG monomeric hinge proteins were mixed in an equimolar ratio (1 μM each) and incubated for 15 min at 16°C. Smc1-SNAP competitor (final concentration 750 nM) was then added to the pre-bound Smc1/Smc3-FLAG mix (final concentration 50 nM) and incubated at 16°C with shaking. An aliquot of this mix was added every 15 min for 90 min to BSA-blocked anti-FLAG beads. Beads were then incubated for 10 min and washed quickly three times. Samples were boiled and run on a 10% SDS–PAGE, transferred by western blotting, and anti-HIS antibody was used to detect Smc proteins. (**C**–**F**) Experiments were performed as described in **B**, but with Smc1/Smc3AAA-FLAG proteins (**C**), Smc1DD/Smc3-FLAG proteins (**D**), Smc1DD/Smc3AAA-FLAG proteins (**E**) or Smc1M665R/Smc3-FLAG proteins (**F**). IN, Input; FT, Flow through; B, Bound fraction.

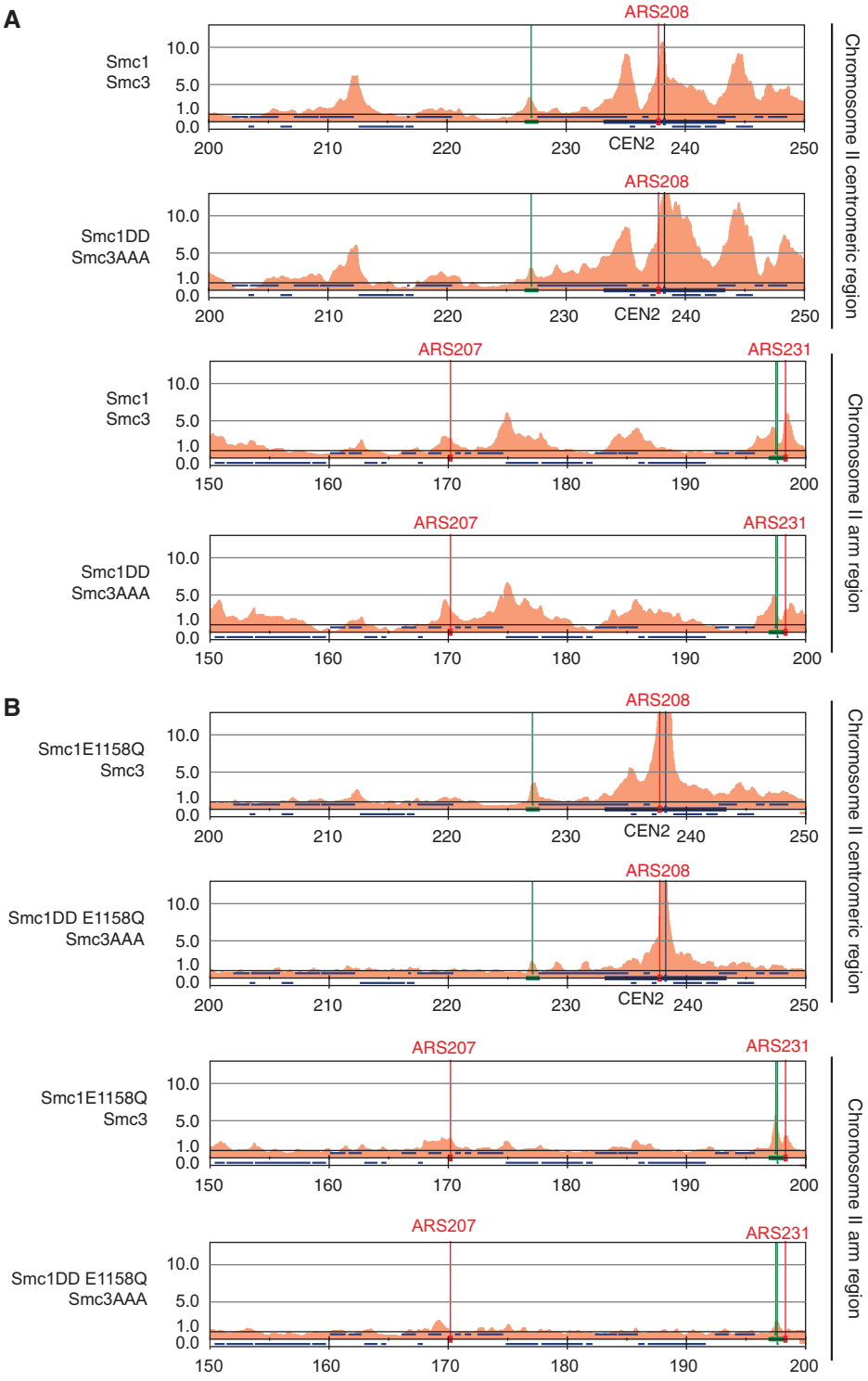

Figure 5 Channel-neutralizing mutations do not affect cohesin's chromosomal distribution genome wide. (**A**) Genome-wide distribution of Smc1-myc9 and Smc1DD-myc9. Cell extracts of cycling cells (K11850; *SMC1-myc9, SMC1, SMC3* and K17075; *smc1DD-myc9, SMC1, smc3AAA*) were used and Smc1-myc9 (Smc1/Smc3) and Smc1DD-myc9 (Smc1DD/Smc3AAA) were immunoprecipitated and processed for ChIP-seq. Binding ratios of 500 bp running windows (50 bp step size) are shown with red bars. Fold enrichment compared with the WCE is plotted on the *y* axis in a linear scale. The *x* axis represents location (kb) along chromosome II. A representative region of 100 kb of chromosome II is depicted (250–150 kb). Average enrichment ratios of mitochondrial and 2 μm DNA were 0.03 and 0.1, respectively, suggesting that all values greater than these represent genuine associations with chromatin. (**B**) Hydrolysis-defective Smc1E1158Q-myc9 and Smc1DDE1158Q-myc9 bind preferentially to the CEN region. Strains K11857 (*smc1E1158Q-myc9, SMC1, SMC3*) and K17037 (*smc1DDE1158Q-myc9, SMC1, smc3AAA*) were prepared and processed as in **A**.

(Supplementary Figure 7A, left panel, Supplementary Figure 7B, top panel). ChIP–qPCR confirmed that there were indeed no major differences in the absolute amount of wild-type and mutant cohesin complexes associated with a variety of loci (Supplementary Figure 7C). The analysis did reveal that Smc1DD-myc9 is slightly more enriched around *CEN* regions

compared with wild-type Smc1-myc9, a conclusion confirmed by ChIP–qPCR (Supplementary Figure 7C, grey and blue bars).

To create sister chromatid cohesion, cohesin must be present during DNA replication (Uhlmann and Nasmyth, 1998). In budding yeast, the entire pool of Scc1 is cleaved at the onset of anaphase and cohesin complexes are only re-generated by a burst of Scc1 synthesis shortly before S phase. If the mutations delayed association, then it might occur too late to build cohesion. To address this, ChIP–qPCR was carried out to measure association of wild-type and mutant complexes with specific DNA sequences at different time periods after release from α-factor-induced G1 arrest. This revealed that the channel-neutralizing mutations had little, if any, effect on the kinetics of association of cohesin with centromeric or peri-centromeric regions (Supplementary Figure 8). To measure association in individual cells, we used fluorescence microscopy to observe formation of GFP foci surrounding kinetochores marked by Mtw1-RFP as cells expressing ectopic Smc1-GFP or Smc1DD-GFP (together with Smc3 or Smc3AAA, respectively) were released from a G1 arrest induced by α-factor. This assay also revealed little difference between wild-type and mutant complexes (Supplementary Figure 9), and we therefore conclude that the latter's inability to form cohesion cannot be due to delayed chromatin association.

We have recently discovered that cohesin complexes whose NBDs can engage but not hydrolyse ATP (such as Smc1E1158Q) are greatly enriched together with Scc2/4 complexes at core centromeres thought to be major sites of cohesin loading (Hu *et al*, 2010). We postulate that such complexes form unstable intermediates at cohesin-loading sites. ChIP-seq revealed that the charge-neutralizing mutations had little or no effect on the formation of these intermediates either at core centromeres or at other loci throughout the genome. A scatter plot comparison of Smc1E1158Q/Smc3 and Smc1DDE1158Q/Smc3AAA revealed that enrichment values around core centromeres were highly correlated, with a coefficient of 0.89 (Supplementary Figure 7A, right panel, Supplementary Figure 7B, lower panel), a conclusion confirmed by quantitative measurements of Smc1E1158Q-myc9 or Smc1DDE1158Q by ChIP–qPCR (Supplementary Figure 7C, brown and red bars). Because Smc1E1158Q-containing complexes associate only in an unstable manner with centromeres, their abundance at these loci probably represents the rate of formation of loading intermediates and it might therefore be easier to detect an effect of hinge channel-neutralizing mutations. That we detect little or no effect also confirms that the rate at which cohesin loads onto chromosomes is largely unaltered by the mutations.

Localization in live cells of cohesin with charge-neutralized hinge channels

To investigate the effect on cohesin localization in live cells, we observed the distribution of wild-type and mutant Smc proteins fused to GFP. The mutant cells expressed untagged Smc1DD from the *SMC1* locus, Smc3AAA-GFP fusion protein from the endogenous *SMC3* locus and Smc3-HA3 from an ectopic locus. An isogenic strain lacking the mutations was used as a wild-type control. Both strains expressed Cnm67-tdTomato, permitting visualization of spindle pole bodies. Diploid cells were grown to exponential phase, immobilized on an agarose pad and observed under live conditions. As previously described (Yeh *et al*, 2008), fluorescence from wild-type Smc3-GFP forms a cylinder-shaped structure in cells with medium-sized buds that have replicated their chromosomes and formed bipolar spindles (witnessed by separated twin tdTomato foci; Figure 6A, left column, arrows). This pattern presumably arises from centromeric and peri-centromeric cohesin from all 32 replicated chromosomes that cluster around pole-to-pole microtubules. The barrel has the appearance of two bars when viewed from the side. Due to localized loss of sister chromatid cohesion, sister kinetochores are pulled apart by $\sim 0.5\,\mu m$, which defines the length of the 'cohesin barrel' (Figure 6A, left column). Some fluorescence possibly arises from cohesin proximal to kinetochores, which does not actually hold sister chromatids together, while the remainder corresponds to cohesin further away from the core centromere/kinetochore, mediating centromeric sister chromatid cohesion (Supplementary Figure 5E). The exact contribution of these two cohesin populations to centromeric barrels in metaphase cells has never been established.

The fluorescence pattern in mutant cells differs in two key aspects. First, separation of spindle pole bodies at an equivalent stage of the cell cycle is invariably greater—the average spindle pole separation in >25 wild-type and mutant cells was 1.4 and 2.1 μm, respectively (Figure 6A and B). Second, fluorescence corresponding to centromeric Smc1DD/Smc3AAA-GFP complexes was split into two half barrels, each circumnavigating pole-to-pole microtubules (as in wild-type). The two barrels are separated from each other, an effect presumably facilitated by the greater spindle pole separation in the mutant (Figure 6A, second column, arrows). Importantly, the patterns of single-mutant Smc1DD/Smc3-GFP or Smc1/Smc3AAA-GFP complexes are similar to wild-type complexes (Figure 6A). Thus, the striking 'split barrel' appearance of Smc1DD/Smc3AAA-GFP complexes depends on the (lethal) combination of *smc1DD* and *smc3AAA* mutations. Importantly, sister Smc1DD/Smc3AAA-GFP barrels are so far apart that the cohesin complexes observed cannot be involved in holding sister chromatids together (Figure 6A and B).

The greater separation of spindle poles in the mutant cells would be readily explained if the *smc3AAA* mutations were partially dominant over *SMC3-HA3* in cells that express (only) Smc1DD, giving rise to sub-lethal cohesion defects. To investigate this cohesion defect, we monitored splitting of *URA3* sequences, which were visualized by the binding of Tet repressor-GFP to a tandem array of Tet operators (Michaelis *et al*, 1997). A strain containing an endogenous copy of *smc1DD* as well as *SMC3* and an ectopic copy of *smc3AAA-HA3* was arrested in metaphase and screened for *URA3* GFP dots. In an isogenic control strain lacking either *smc1* or *smc3* mutations, 4% of metaphase-arrested cells contain split dots, but this value increased to 35% in cells harbouring both *smc3AAA* and *smc1DD* mutations. The corresponding values in *smc1DD/SMC3* and *SMC1/smc3AAA* single-mutant cells were 14 and 17%, respectively (Supplementary Figure 5D). We conclude that Smc3AAA interferes with the ability of Smc1DD/Smc3 heterodimers in conferring sister chromatid cohesion, an effect that may be, at least partly, caused by the fact that dysfunctional Smc1DD/Smc3AAA dimers are more stable than functional Smc1DD/Smc3 dimers.

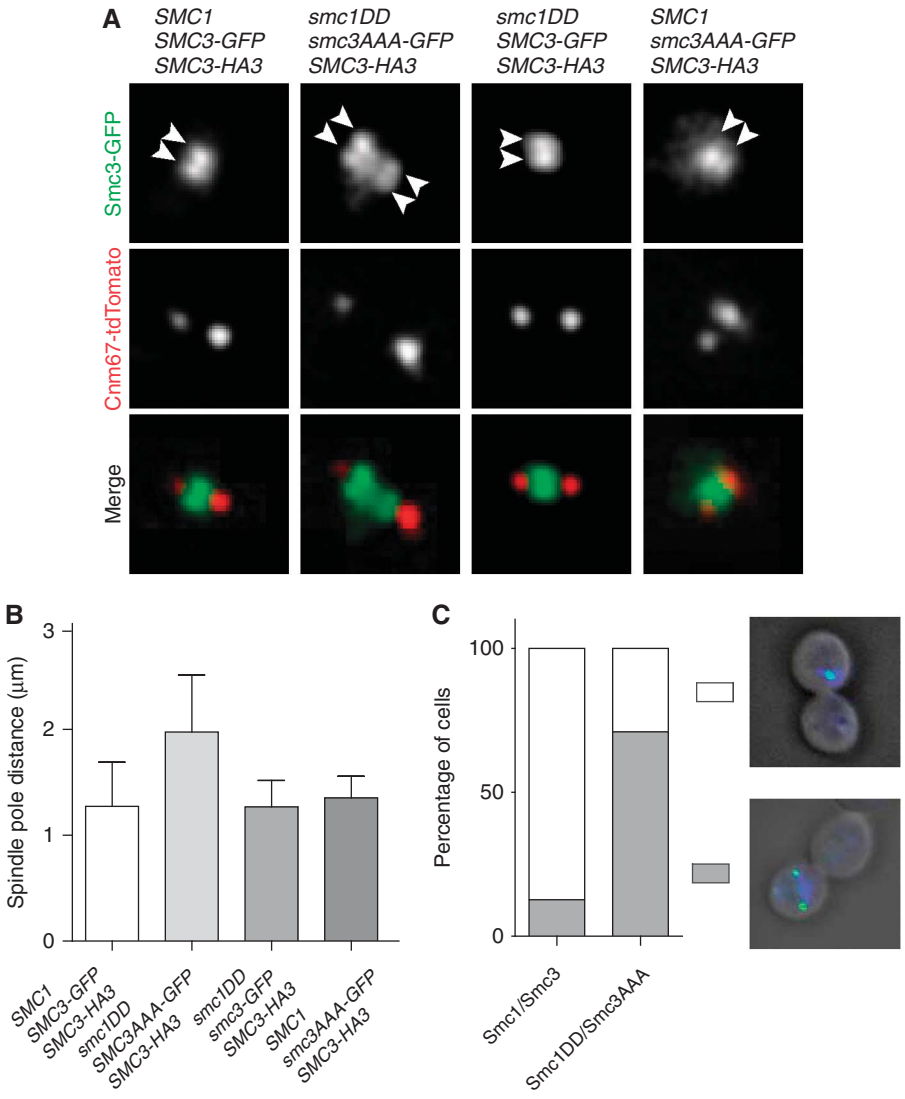

Figure 6 Channel-neutralized cohesin forms distinct split barrel structures. (**A**) Smc3-GFP forms a cylindrical structure between marked spindle poles (Cnm67-tdTomato), as observed previously (Yeh *et al*, 2008) in wild-type cells (K15927; *SMC3-GFP, SMC1, SMC3-HA3; left column*). The second column represents mutant cells harbouring *smc1DD* and *smc3AAA-GFP* mutations (K15947), showing elongated spindles and two cylindrical structures near poles. The third and fourth columns represent the biologically viable single-mutant combinations *smc1DD/SMC3-GFP* (K16122) and *smc3AAA-GFP/SMC1* (K15990), respectively, forming wild-type barrel structures. White arrowheads indicate barrel structure. (**B**) Spindle pole distances are increased in charge-neutralized mutants. Average spindle pole distance in medium-budded cells for wild-type (K15927) control strain and mutant (K15947, K16122, K15990) strains was plotted. Cnm67-tdTomato was used as spindle pole marker; $n = 25$, $P < 0.001$, error bars = s.d. (**C**) Neutralization of the hinge channel induces drastic loss of sister chromatid cohesion in metaphase-arrested cells. Wild-type Smc1/Smc3 (K16901; *SMC1, SMC3-HA3, smc3-42, ura3::3xURA3 tetO112; tetR-GFP, MET-CDC20*) and hinge-neutralized mutant cells Smc1DD/Smc3AAA (K16906; *smc1DD, smc3AAA-HA3, smc3-42, ura3::3xURA3 tetO112; tetR-GFP, MET-CDC20*) were arrested in metaphase by Cdc20 depletion in Met-containing media for 1 h at 25°C. Cells were then shifted up to 35°C to inactivate *smc3-42*. After complete arrest (3 h), cells were fixed and sister chromatid cohesion was monitored by Tet operator/repressor-GFP dots at the *URA3* locus by fluorescence microscopy; $n = 100$ cells.

Cohesin complexes with neutralized hinge channels associate stably with peri-centromeric chromatin

To compare the stability of wild-type and mutant complexes associated with centromeric barrels in metaphase cells, we measured the effect of repeatedly photobleaching a neighbouring zone within the same nucleus, a technique known as fluorescence loss in photobleaching (FLIP). We chose this method in preference to the technique known as fluorescence recovery after photobleaching (FRAP) for two reasons. First, it is difficult to bleach precisely one half of wild-type cohesin barrels in metaphase cells and second, centromere mobility, especially in the case of mutant cells, would compromise FRAP estimates of stability. Because the fluorescence of unbleached barrels (either wild-type or mutant) does not change appreciably during this cell cycle window (Supplementary Figure 10A and B), we assume that chromatin-bound and soluble pools are in steady state. If cohesin within centromeric barrels exchanges rapidly with the soluble pool, then fluorescence associated with barrels should be eliminated by repeated bursts of photobleaching a neighbouring zone. However, if not, it should persist. Diploid yeast strains were plated onto YEPD agar pads and a single spot within the nucleus outside the barrel-shaped structure was repeatedly bleached. One pre-bleach image was collected and

then images were captured after each bleach pulse, with 2 s between bleach pulses, for 90 s. To avoid damage of the cell and activation of the spindle assembly checkpoint by excessive laser usage, subsequent images were acquired without bleach pulses every 60 s for a total of 460 s (the chase period). Fluorescence loss of the unbleached barrel-shaped structure was measured for every time point, corrected for photobleaching and for background fluorescence and relative fluorescence intensity (RFI) plotted against time.

To validate our FLIP protocol, we compared RFI graphs of wild-type Smc3-GFP before and just after cells had undergone anaphase, when Scc1 cleavage releases cohesin from chromosomes. RFI of Smc3-GFP/Smc1 complexes drops rapidly to background levels during the bleaching period in post-anaphase cells and does not thereafter recover, suggesting that cohesin complexes cleaved by separase diffuse rapidly in and out of the zone subjected to photobleaching. In metaphase cells, in contrast, RFI declines by at most 40% during the 90-s bleaching period (Figure 7A). The kinetics of this decline suggests that it is due to collateral photobleaching (a linear process) as well as bleaching of a background soluble pool (an exponential process). The RFI thereafter remains constant during the entire chase period. These measurements imply that a large fraction of the cohesin associated with the barrels never enters the bleached zone and must therefore be stably associated with chromatin. Importantly, RFIs associated with Smc3-AAA-GFP/Smc1DD complexes in metaphase cells have very similar kinetics to wild type (Figure 7A and Supplementary Figure 10C). Our FLIP experiments imply that the hinge charge-neutralizing mutations have little measurable effect on the stability of cohesin's association with chromatin. A corollary is that association with chromatin cannot *per se* be responsible for the lack of sister chromatid cohesion associated with these mutations.

Defective acetylation of cohesin complexes with neutralized hinge channels during S phase

If the hinge channel-neutralizing mutations have no major effect on the rate, distribution or stability of cohesin's association with chromatin, why then do they so comprehensively abolish sister chromatid cohesion? A crucial event in establishing cohesion is acetylation by the Eco1 acetyltransferase of a pair of lysine residues (K112 and K113) on the surface of the Smc3's NBD (Ben-Shahar *et al*, 2008; Rowland *et al*, 2009; Unal *et al*, 2008), which occurs during S phase and is maintained until anaphase when it is removed by the Hos1 de-acetylase (Beckouët *et al*, 2010; Borges *et al*, 2010). To investigate whether Smc3 acetylation is affected, we used strains expressing either Smc1-myc9 and Smc3-HA3 or Smc1DD-myc9 and Smc3AAA-HA3 from ectopic loci together with untagged Smc3 from its endogenous locus. Crude extracts were prepared from exponentially grown cells, epitope-tagged Smc3 immunoprecipitated using HA-specific antibodies and western blots probed either with antibodies specific for acetylated K113 or for the HA epitope. This revealed that Smc3 K113 acetylation of Smc1DD/Smc3AAA complexes is on average five- to sixfold less than wild type (Figure 7B). Acetylation of the viable Smc1/Smc3AAA and Smc1DD/Smc3 was also reduced, albeit much less so. Crucially, no Smc3 acetylation was detected when Smc3-HA3 was immunoprecipitated from Δ*rad61*/Δ*eco1* cells (Ben-Shahar *et al*, 2008; Rowland *et al*, 2009) lacking the acetyltransferase.

To address whether the reduced acetylation is due to defective acetylation during S phase, as opposed to a failure to maintain acetylation during G2/M phase, we analysed synchronous cultures. Cells with Cdc20 under control of the MET3 promoter were first arrested in metaphase by Cdc20 depletion, released into G1 by transferring cells into synthetic medium lacking Met (allowing Cdc20 expression) but containing α-factor pheromone and finally stimulated to enter S phase and re-arrest in metaphase by transferring cells to complete medium containing Met but lacking pheromone (Figure 7C). K113 acetylation associated with Smc1/Smc3 complexes rises rapidly as cells enter S phase and persists at high levels thereafter. In contrast, acetylation associated with Smc1DD/Smc3AAA complexes barely rose as cells entered S phase and remained low as cells re-accumulated in metaphase, suggesting a defect in *de novo* Smc3 acetylation. Further evidence for this conclusion is the observation that the *smc1DD/smc3AAA* mutations reduce Smc3 acetylation in Δ*hos1* cells to an extent similar to that seen in *HOS1* cells (Figure 7D). Inactivation of Hos1 caused a 1.8-fold increase in acetylation of wild-type complexes and a 2.1-fold increase in Smc1DD/Smc3AAA complexes. Interestingly, the latter is not accompanied by restoration of viability (data not shown), either because acetylation is not the only lethal defect in *smc1DD/smc3AAA* cells and/or because Smc3 molecules that are not de-acetylated at anaphase in Δ*hos1* cells cannot build cohesion during the next S phase (Beckouët *et al*, 2010). Decreased acetylation of Smc3 cannot be the sole cause of the lethality associated with hinge channel-neutralizing mutations, as their lethality is not suppressed by inactivation of Rad61 (data not shown), which is known to suppress loss of Eco1 (Ben-Shahar *et al*, 2008; Beckouët *et al*, 2010; Borges *et al*, 2010).

Discussion

The structure of the murine Smc1/Smc3 hinge domain is very similar to that of the homodimeric hinge domain from *T. maritima*. In both cases, shallow U-shaped hinge monomers interact to form a twofold symmetric torus containing a small positively charged channel through the middle. A cluster of (non-conserved) lysine residues has been previously described on the outer surface of the *Bacillus subtilis* SMC hinge (Hirano and Hirano, 2006; Supplementary Figure 3C). Modelling shows that the lysine side chains do not point inside the SMC hinge channel, and mutating these residues to aspartic acid is predicted to abolish the overall positive charge on the outside of the *B. subtilis* hinge without affecting the charge inside the channel (Supplementary Figure 3A and B). In contrast to the positive charges within the channel, outer surface charges are not conserved amongst prokaryotic and eukaryotic SMC hinges (Supplementary Figures 1 and 2). The channel arises as a consequence of the bipartite nature of the dimerization domain, with semi-independent 'north' and 'south' interfaces. Mutations in Smc1 (Smc1DD) and Smc3 (Smc3AAA) that together largely neutralize the channel's charges are lethal when combined. One possible trivial explanation for this lethality is that the cluster of neutralizing mutations reduces the affinity of half hinges, which according to the ring model would accelerate dissociation of cohesin from chromatin. *In vitro* binding studies with isolated hinge

domains show that the dissociation constant (K_d) is not greatly altered by neutralizing mutations. However, K_{off} is reduced (by an order of magnitude or more) and by implication, K_{on} must also be reduced. Crucially, co-precipitation studies using cell extracts demonstrate that full-length Smc1DD forms dimers with Smc3AAA as efficiently as wild-type Smc1, even when competing for a limiting amount of Smc3 protein. Cohesin rings are formed with wild-type efficiency *in vivo* (despite the presumed reduction in K_{on}), and once formed, the mutant hinge interface is less, not more, likely to dissociate transiently than wild type. Neither deficient Smc1/Smc3 heterodimerization, leading to a lack of cohesin rings, nor a failure to maintain a stable association between Smc1 and Smc3, which is known to compromise cohesion (Mishra *et al*, 2010), can be the cause of Smc1DD/Smc3AAA hinge dysfunction. These findings prove that cohesin's hinge has a crucial activity destroyed by the channel-neutralizing mutations besides high-affinity Smc1/Smc3 dimerization.

What might this activity be? Our data suggest that it is not the loading of cohesin onto chromosomes *per se*. Cohesin complexes with hinge channel-neutralizing mutations associate stably with chromatin with apparently normal kinetics and have a very similar genomic distribution to wild-type complexes. If stable association with chromosomes involves entrapment of chromatin fibres inside cohesin rings and if

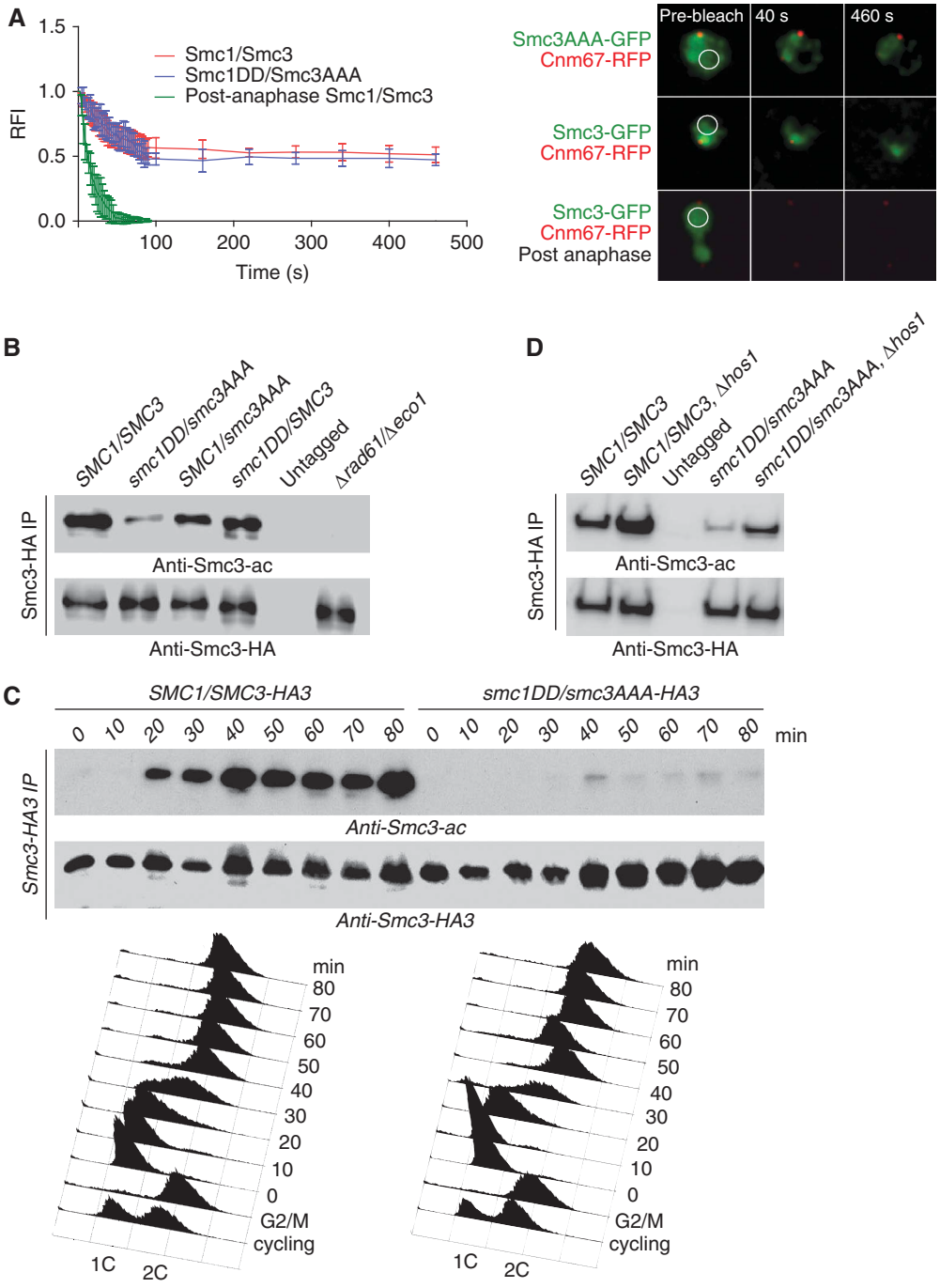

this process involves transient hinge dissociation (Gruber *et al*, 2006), then the positive charge of the hinge's narrow channel cannot be required for dissociation *per se*, despite the fact that neutralization reduces K_{off}, at least *in vitro*. Our work also suggests that the pathology caused by the hinge channel charge-neutralizing mutations does not stem from any obvious effect on the stability of cohesin's association with chromosomes, as FLIP experiments suggest that this is unaltered.

Our results point instead to the defect caused by the hinge channel charge-neutralizing mutations being a highly specific one that affects the process by which cohesin that has already associated with chromatin manages to entrap sister DNAs following the passage of replication forks. Our finding that the positively charged residues within the hinge interface are required for cohesion establishment and for efficient acetylation of Smc3 NBDs, but not for stable association with chromatin *per se*, can only be explained if the hinge participates in a major conformational change that accompanies the entrapment of sister chromatin fibres during S phase. The ring model envisages two main scenarios by which this comes about: either rings that have already entrapped unreplicated chromatin fibres are converted during passage of replication forks to ones that entrap sister fibres or the rings that entrap sister fibres are derived from a soluble pool and must re-load onto chromatin at the time of replication. In the case of the first scenario, the replication apparatus either passes through rings that remain shut once they have associated with unreplicated chromatin or rings associated with unreplicated chromatin re-open during passage of the fork while remaining associated with the replicating chromatin fibre. Whichever scenario is correct, the stable entrapment of sister DNAs is accompanied by and dependent on *de novo* acetylation of Smc3 NBDs, which has been suggested to lock rings shut (Beckouët *et al*, 2010).

There are, in principle, three types of explanation for the phenotypes caused by the hinge channel charge-neutralizing mutations. According to the first, establishment of cohesion is necessary for acetylation of Smc3 by Eco1, and the deficient acetylation is an indirect effect resulting from a failure to create cohesive structures (Figure 8A). The problem with this explanation is that if Smc3 acetylation measures formation of cohesive structures, then Smc1DD/Smc3AAA complexes should produce as much, if not more, cohesion as *eco1-1* mutants grown at the permissive temperature, which they clearly do not (Rowland *et al*, 2009). In other words, this scenario cannot explain why their defective cohesion is more severe than their defective acetylation. The second explanation

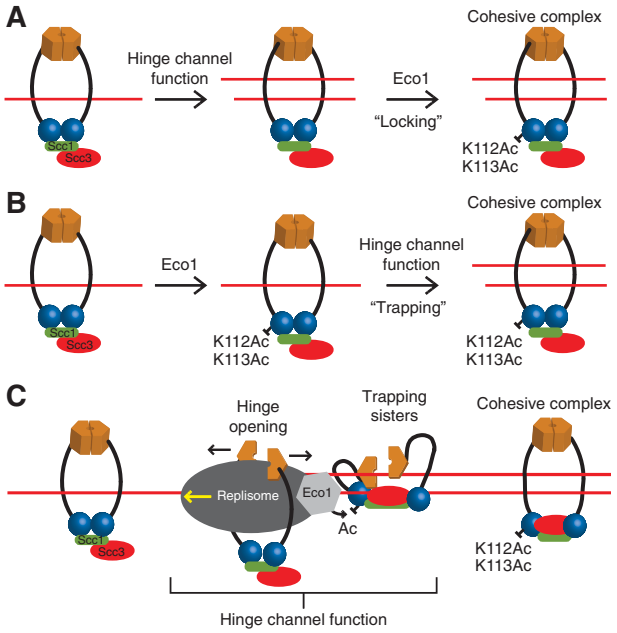

Figure 8 Models of hinge channel function. (**A**) Model 1. Establishment of cohesion requires first hinge function to allow sister chromatid entrapment. Eco1 acetylates only cohesed sisters, thereby locking them into a stable DNA–protein complex. (**B**) Model 2. Only when the Smc3 NBD is acetylated, trapping of both sisters occurs by means of the hinge function. (**C**) Model 3. Cohesin associates with DNA at the onset of S phase by embracing single-stranded DNA or through a stable physical DNA–protein interaction. Cohesin hinge domains open to allow passage of the replisome. Transient association of the hinge domains with the Smc3 NBD stimulates acetylation, which then allows re-shutting of the hinge domains and formation of stable rings around sister chromatids. Acetylation locks cohesin in a stable structural state, possibly with heads disengaged to prevent opening of the ring by ATP hydrolysis.

Figure 7 Charge neutralization in the hinge channel does not change cohesin's stable association with chromatin, but reduces acetylation of Smc3AAA protein. (**A**) Smc3AAA-GFP/Smc1DD complex associates stably with chromatin in G2/M. FLIP experiments were performed with a 488 nm laser bleaching the nuclear GFP signal. Fluorescence of the barrel-shaped structure was measured in medium-budded cells of wild-type strain K15927 (*SMC3-GFP, SMC1, SMC3-HA3*) every 2 s after each bleach pulse for 90 s, and thereafter at every 60 s without bleach pulses for a total of 460 s. Selected images of a single FLIP experiment using Smc3-GFP are shown (right panel). FLIP of Smc3AAA-GFP (K15947; *smc3AAA-GFP, smc1DD, SMC3-HA3*) in G2/M cells and wild-type Smc3-GFP in post-anaphase cells (K15927) was performed in the same way. Relative fluorescence intensities of Smc3-GFP or Smc3AAA-GFP were plotted over time. Circles indicate bleaching area ($n = 10$, error bars = s.d.). (**B**) Acetylation of Smc3AAA protein is reduced in charge-neutralized hinge mutant. Crude extract from exponentially growing strains K16270 (*SMC1-myc9, SMC3, SMC3-HA3*), K15280 (*smcDD1-myc9, SMC3, smc3AAA-HA3*), K17419 (*SMC1-myc9, SMC3, smc3AAA-HA3*), K17420 (*smc1DD-myc9, SMC3, SMC3-HA3*), K15794 (Δ*rad61*/Δ*eco1, SMC3, SMC3-HA3*) and an untagged strain (K15278) were prepared and Smc3-HA3 proteins were immunoprecipitated. Proteins were visualized by western blot using either 3F10 (anti-HA antibody) or antibodies against Smc3-ac. (**C**) Smc3AAA acetylation is decreased in S phase. Wild-type strain K17328 (*SMC1-myc9, SMC3-HA3, SMC3, MET-CDC20*) and mutant strain K17329 (*smc1DD-myc9, smc3AAA-HA3, SMC3, MET-CDC20*) were first arrested in metaphase by Cdc20 depletion in Met-containing medium for 2 h at 30°C. Cells were then released into α-factor-containing medium, arrested for 1 h and again released into Met-containing medium for second metaphase arrest. Samples were taken every 10 min after G1 release and processed for Smc3-HA3 immunoprecipitation. Smc3-HA3 proteins and Smc3-ac proteins were visualized by western blotting using 3F10 and anti-Smc3-ac antibodies, respectively. FACS profile shows cell progression throughout the cell cycle by monitoring DNA content. (**D**) Deleting the deacetylase *HOS1* increases acetylation of Smc3 proteins. Experiment was carried out as in **B** using strains K17325 (*SMC1-myc9, SMC3-HA3, SMC3, HOS1*), K17630 (*SMC1-myc9, SMC3-HA3, SMC3,* Δ*hos1*), K699 (untagged), K17326 (*smc1DD-myc9, smc3AAA-HA3, SMC3, HOS1*) and K17699 (*smc1DD-myc9, smc3AAA-HA3, SMC3,* Δ*hos1*). Acetylation increases, in average, by 1.8 ± 0.2-fold ($n = 3$) in Δ*hos1* cells (*SMC1/SMC3,* Δ*hos1*) compared with wild-type cells (*SMC1/SMC3, HOS1*) and by 2.1 ± 0.2-fold ($n = 3$) in Δ*hos1* channel-neutralized mutant cells (*smc1DD/smc3AAA,* Δ*hos1*) compared with channel-neutralized mutant cells harbouring the *HOS1* gene (*smc1DD/smc3AAA, HOS1*).

envisages a reversed chain of causality, namely, the cohesion defects caused by the mutant hinges are in fact a consequence not a cause of the deficient Smc3 acetylation (Figure 8B). However, this explanation is also inadequate, because it cannot explain why deletion of *RAD61*, which is known to suppress the lethality of *eco1*Δ mutations (Rowland *et al*, 2009), does not suppress that of *smc1DD/smc3AAA* mutants. In other words, defective cohesion is not caused solely by defective Smc3 acetylation.

This leads us to favour a third scenario according to which Smc3 NBD acetylation and establishment of cohesive structures, which we presume to be co-entrapment of sister DNAs inside cohesin rings, are both aspects of a concerted process involving a major conformational change in the structure of the hinge that is adversely affected by the hinge channel-neutralizing mutations. Because the mutated residues are largely buried when hinges are fully closed, we suggest that this conformational change involves partial or even complete hinge dissociation. Because the hinge is separated from Smc3's NBD by a 50-nm long albeit broken coiled coil, we propose that it involves the transient association of hinge domains with the Smc3 NBD, whose acetylation is stimulated by them. If establishment of cohesion at replication forks requires the transient re-opening of cohesin rings, then re-opening itself and/or shutting re-opened rings must be coordinated with acetylation of Smc3 NBDs and possibly requires a fresh ATP-binding/hydrolysis cycle (Figure 8C). Whether the decreased K_{on} or K_{off} of the mutant hinges contributes to their defect is currently unclear. Future studies will be required to reveal the role of positive charges within bacterial and condensin Smc hinge domains. It is admittedly difficult to reconcile our suggestion that the positive charge inside cohesin's hinge is concerned with events that occur at replication forks with the notion that condensin only acts during mitosis. One possibility is that the sort of conformational change that occurs to cohesin during replication takes place during mitosis in the case of condensin. Another possibility is that by introducing mutations designed to remove its positive charge, we have inadvertently altered some other crucial aspect of the cohesin hinge's function. In other words, the phenotypes are not caused by neutralization *per se*. Irrespective of the precise mechanism, our results imply an unexpected involvement of residues buried within the hinge interface in a major conformational change of the cohesin complex during S phase that is required both for Smc3 acetylation and the establishment of sister chromatid cohesion. Cohesin's hinge is therefore not merely a dimerization domain.

Materials and methods

Expression and purification of the mouse Smc1/Smc3 hinge dimer

Sequences encoding amino acids 484–696 of *M. musculus* Smc3 (NP_031816.2) and sequences encoding amino acids 471–685 of *M. musculus* Smc1 (NP_062684.1) fused to a C-terminal 6xHis tag were cloned by PCR into the pET28 expression vector. Expression of Smc1/Smc3 hinge domains was induced by addition of 0.25 mM IPTG for 5 h at 30°C in *E. coli* strain BL21(DE3)-RIPL (Stratagene). Cells were lysed in 50 mM sodium phosphate buffer (pH 8.0) with 300 mM NaCl and Complete EDTA-Free Protease Inhibitor Mix (Roche). The complex was purified using Ni^{2+}-chelating affinity chromatography followed by size-exclusion chromatography in TEN buffer (20 mM Tris–HCl (pH 8.0), 1 mM EDTA, 1 mM NaN_3, 100 mM NaCl and 2 mM DTT).

For the production of SeMet-substituted protein, cells were grown in supplemented M9 media (van den Ent *et al*, 2006) and induced with 0.25 mM IPTG for 13 h at 16°C. The Smc1/Smc3 dimer was purified as described above, except that 5 mM BME was added to all buffers for the Ni^{2+} column and 5 mM DTT was used in the size-exclusion chromatography buffer.

M. musculus Smc1/Smc3 hinge domain heterodimer crystal structures

For crystallization, an initial screening was performed according to Stock *et al* (2005). Native crystals were produced using sitting-drop vapour diffusion at 19°C with 200 nl of 27 mg/ml protein in TEN buffer and 200 nl of precipitant solution containing 200 mM Li_2SO_4, 100 mM Tris (pH 8.5), 30% PEG 3000, and equilibrated against the latter for 4 days. Crystals were frozen in precipitant solution plus 15% glycerol, and data were collected at beamline ID23eh1 at ESRF, Grenoble, France. SeMet crystals were produced using 500 nl of 27 mg/ml protein in TEN buffer and 162 nl of precipitant solution (2 M $(NH_4)_2SO_4$, 100 mM Tris (pH 8.5)), and equilibrated against the latter for 4 days. Crystals were frozen in precipitant solution plus 15% glycerol. A SAD data set was collected at the peak wavelength for selenium at the same beamline. All data were processed and reduced using the CCP4 program (1994). Molecular replacement using PHASER (McCoy, 2007) and two *T. maritima* SMC hinge monomers (PDB 1GXK) produced a clear solution showing a similar dimer arrangement. Unambiguous assignment of Smc1 and Smc3 was facilitated by the location of eight selenium positions in an anomalous Fourier map using molecular replacement model phases and the SeMet anomalous differences collected at the peak wavelength. Model building was done using MAIN (Turk, 2000) and refinement was performed using PHENIX.refine (Adams *et al*, 2002). The structure has been deposited in the PDB (1WD5).

Yeast strains

Strains used are derived from W303 and are listed in Supplementary Table 3. All yeast strains were grown at 30°C in YEPD unless stated otherwise.

Protein purification and binding assays

smc3AAA and *smc1DD* mutants were derived by site-directed mutagenesis (Stratagene). To *SMC1* and *SMC3* hinge sequences of *S. cerevisiae* (*SMC1 S480-E681*, *SMC3 T495-L695*) a C-terminal 6xHis tag and an N-terminal MBP were fused, and sequences were then cloned into pMAL expression vector (NEB). Expression and purification was performed as previously described (Mishra *et al*, 2010).

Co-immunoprecipitation assay

Experiment was carried out as described previously (Arumugam *et al*, 2003; Beckouët *et al*, 2010).

Isothermal titration calorimetry

Calorimetric measurements were performed with Smc1 and Smc3 using a VP-ITC titration calorimeter (MicroCal Inc.). Each experiment was initiated with an injection volume of 2 μl of Smc3 (100 μM) followed by 29 injections of 10 μl into a solution of 10 μM Smc1 protein. Origin software (MicroCal Inc.) was used for evaluation.

In vivo competition assay

Strains were grown in 2 l YEP media with 2% glucose to $OD_{595\,nm} = 1.6$. Cells were harvested and lysed in lysis buffer (50 mM Tris–HCl (pH 7.5), 250 mM NaCl, 1 mM PMSF, 1% Triton X-100) by means of a French Press (Constant System, Northants, UK). Cleared lysate was then incubated for 2 h in 3F10-coupled agarose beads (Roche), the beads were washed three times with lysis buffer and the protein was analysed by SDS–PAGE and silver staining.

Ligand competitor experiment

Hinge proteins were expressed and purified as described above. Smc1 and Smc3-FLAG were mixed in an equimolar ratio (1 μm each, Mix 1) in buffer 1 (20 mM HEPES (pH 7.5), 90 mM NaCl, 2 mM BME, 1% Triton X-100) and incubated for 15 min at 16°C. Mix 1 (final concentration 50 nM) was added to a tube containing Smc1-SNAP competitor (final concentration 750 nM) and incubated at 16°C

with shaking. Of this solution, 250 µl was added every 15 min to BSA-blocked anti-FLAG beads (Sigma-Aldrich). Beads were then incubated for 10 min and washed three times with buffer 1. Boiled samples were analysed by western blotting using anti-HIS antibody (Qiagen).

Chromatin immunoprecipitation-quantitative PCR

ChIP–qPCR assays were performed as described (Gruber *et al*, 2006) using 2 µg of 9E11 anti-myc antibody.

Fluorescence microscopy and FLIP experiments

Cells were imaged with a wide-field spinning disk imaging system (PerkinElmer) based on an Olympus IX 7 instrument. Images were acquired at 25°C using Volocity imaging software. For quantitative analysis of Smc3-GFP, cells were grown to log phase in YEPD. After immobilization on 2.5% agarose pads, medium-budded cells were picked and single stack images were acquired. FLIP was performed by pulse bleaching (488 nm, 30 ms, 5% laser intensity, spot diameter ~700 nm) with a ×100 lens.

Quantitative analysis was carried out with ImageJ 1.44v software. After correction for photobleaching, the RFI was calculated using the following equation (Dundr and Misteli, 2003):

$$\mathrm{RFI} = \frac{\left(I_{\mathrm{u}\,t_0} - I_{\mathrm{Bg}\,t_0}\right)}{\left(I_{\mathrm{u}\,t_\infty} - I_{\mathrm{Bg}\,t_\infty}\right)}$$

where I_{u} is the mean intensity of the unbleached area and I_{Bg} the mean intensity of the background.

Supplementary data

Supplementary data are available at *The EMBO Journal* Online (http://www.embojournal.org).

Acknowledgements

We are grateful to Nasmyth lab members for useful discussions, R Parton and I Dobbie for help with microscopy and K Bloom for providing the Smc3-GFP tagging plasmid. AK and KN were supported by Cancer Research UK and the Wellcome Trust.

Author contributions: AK and KN wrote the paper; AK, AM, CHH and KN designed the experiments; CHH and KAM carried out modelling; CHH and LS expressed and purified the mouse hinge protein; KAM and JL solved the crystal structure; SED carried out Koff experiment under the supervision of AK; SK designed and carried out MD simulations; TI and KS carried out and analysed ChIP-seq experiments; and AK performed all other experiments.

Conflict of interest

The authors declare that they have no conflict of interest.

References

Adams PD, Grosse-Kunstleve RW, Hung LW, Ioerger TR, McCoy AJ, Moriarty NW, Read RJ, Sacchettini JC, Sauter NK, Terwilliger TC (2002) PHENIX: building new software for automated crystallographic structure determination. *Acta Crystallogr D Biol Crystallogr* **58**(Part 11)**:** 1948–1954

Arumugam P, Gruber S, Tanaka K, Haering CH, Mechtler K, Nasmyth K (2003) ATP hydrolysis is required for cohesin's association with chromosomes. *Curr Biol* **13:** 1941–1953

Arumugam P, Nishino T, Haering CH, Gruber S, Nasmyth K (2006) Cohesin's ATPase activity is stimulated by the C-terminal winged-helix domain of its kleisin subunit. *Curr Biol* **16:** 1998–2008

Beckouët F, Hu B, Roig MB, Sutani T, Komata M, Uluocak P, Katis VL, Shirahige K, Nasmyth K (2010) An Smc3 acetylation cycle is essential for establishment of sister chromatid cohesion. *Mol Cell* **39:** 689–699

Ben-Shahar TR, Heeger S, Lehane C, East P, Flynn H, Skehel M, Uhlmann F (2008) Eco1-dependent cohesin acetylation during establishment of sister chromatid cohesion. *Science* **321:** 563–566

Borges V, Lehane C, Lopez-Serra L, Flynn H, Skehel M, Ben-Shahar TR, Uhlmann F (2010) Hos1 deacetylates Smc3 to close the cohesin acetylation cycle. *Mol Cell* **39:** 677–688

CCP program (1994) The CCP4 suite: programs for protein crystallography. *Acta Crystallogr D Biol Crystallogr* **50**(Part 5)**:** 760–763

Ciosk R, Shirayama M, Shevchenko A, Tanaka T, Toth A, Shevchenko A, Nasmyth K (2000) Cohesin's binding to chromosomes depends on a separate complex consisting of Scc2 and Scc4 proteins. *Mol Cell* **5:** 243–254

Dundr M, Misteli T (2003) Measuring dynamics of nuclear proteins by photobleaching. *Curr Protoc Cell Biol*, Chapter 13, Unit 13.5

Griese JJ, Witte G, Hopfner KP (2010) Structure and DNA binding activity of the mouse condensin hinge domain highlight common and diverse features of SMC proteins. *Nucleic Acids Res* **38:** 3454–3465

Gruber S, Arumugam P, Katou Y, Kuglitsch D, Helmhart W, Shirahige K, Nasmyth K (2006) Evidence that loading of cohesin onto chromosomes involves opening of its SMC hinge. *Cell* **127:** 523–537

Gruber S, Haering CH, Nasmyth K (2003) Chromosomal cohesin forms a ring. *Cell* **112:** 765–777

Haering CH, Farcas A, Arumugam P, Metson J, Nasmyth K (2008) The cohesin ring concatenates sister DNAs. *Nature* **454:** 297–301

Haering CH, Lowe J, Hochwagen A, Nasmyth K (2002) Molecular architecture of SMC proteins and the yeast cohesin complex. *Mol Cell* **9:** 773–788

Hauf S, Waizenegger IC, Peters JM (2001) Cohesin cleavage by separase required for anaphase and cytokinesis in human cells. *Science* **293:** 1320–1323

Hirano M, Hirano T (2002) Hinge-mediated dimerization of SMC protein is essential for its dynamic interaction with DNA. *EMBO J* **21:** 5733–5744

Hirano M, Hirano T (2006) Opening closed arms: long-distance activation of SMC ATPase by hinge-DNA interactions. *Mol Cell* **21:** 175–186

Hu B, Itoh T, Mishra A, Katoh Y, Chan K-L, Upcher W, Godlee C, Roig MB, Shirahige K, Nasmyth K (2010) Identification of an intermediate step in the cohesin chromosome loading reaction. *Curr Biol* (in press)

Ivanov D, Schleiffer A, Eisenhaber F, Mechtler K, Haering CH, Nasmyth K (2002) Eco1 is a novel acetyltransferase that can acetylate proteins involved in cohesion. *Curr Biol* **12:** 323–328

Ku B, Lim JH, Shin HC, Shin SY, Oh BH (2010) Crystal structure of the MukB hinge domain with coiled-coil stretches and its functional implications. *Proteins* **78:** 1483–1490

Li Y, Schoeffler AJ, Berger JM, Oakley MG (2010) The crystal structure of the hinge domain of the *Escherichia coli* structural maintenance of chromosomes protein MukB. *J Mol Biol* **395:** 11–19

McCoy AJ (2007) Solving structures of protein complexes by molecular replacement with Phaser. *Acta Crystallogr D Biol Crystallogr* **63**(Part 1)**:** 32–41

Melby TE, Ciampaglio CN, Briscoe G, Erickson HP (1998) The symmetrical structure of structural maintainance of chromosomes (SMC) and MukB proteins: long, antiparallel coiled coils, folded at a flexible hinge. *J Cell Biol* **142:** 1595–1604

Michaelis C, Ciosk R, Nasmyth K (1997) Cohesins: chromosomal proteins that prevent premature separation of sister chromatids. *Cell* **91:** 35–45

Mishra A, Hu B, Kurze A, Beckouet F, Farcas AM, Dixon SE, Katou Y, Khalid S, Shirahige K, Nasmyth K (2010) Both interaction surfaces within cohesin's hinge domain are essential for its stable chromosomal association. *Curr Biol* **20:** 279–289

Nasmyth K, Haering CH (2005) The structure and function of SMC and kleisin complexes. *Annu Rev Biochem* **74:** 595–648

Rowland BD, Roig MB, Nishino T, Kurze A, Uluocak P, Mishra A, Beckouët F, Underwood P, Metson J, Imre R, Mechtler K, Katis VL, Nasmyth K (2009) Building sister chromatid cohesion: Smc3 acetylation counteracts an antiestablishment activity. *Mol Cell* **33:** 763–774

Skibbens RV, Corson LB, Koshland D, Hieter P (1999) Ctf7p is essential for sister chromatid cohesion and links mitotic

chromosome structure to the DNA replication machinery. *Genes Dev* **13:** 307–319

Stock D, Perisic O, Lowe J (2005) Robotic nanolitre protein crystallisation at the MRC laboratory of molecular biology. *Prog Biophys Mol Biol* **88:** 311–327

Toth A, Ciosk R, Uhlmann F, Galova M, Schleiffer A, Nasmyth K (1999) Yeast cohesin complex requires a conserved protein, Eco1p(Ctf7), to establish cohesion between sister chromatids during DNA replication. *Genes Dev* **13:** 320–333

Turk D (2000) MAIN 96: an interactive software for density modifications, model building, structure refinement and analysis. In *Crystallographic Computing 7: Macromolecular Crystallographic Data (Crystallographic Computing)*, Bourne PE, Watenpaugh K (eds). Oxford: Oxford University Press

Uhlmann F, Lottspeich F, Nasmyth K (1999) Sister chromatid separation at anaphase onset is promoted by cleavage of the cohesin subunit Scc1p. *Nature* **400:** 37–42

Uhlmann F, Nasmyth K (1998) Cohesion between sister chromatids must be established during DNA replication. *Curr Biol* **8:** 1095–1101

Uhlmann F, Wernic D, Poupart MA, Koonin E, Nasmyth K (2000) Cleavage of cohesin by the CD clan protease separin triggers anaphase in yeast. *Cell* **103:** 375–386

Unal E, Heidinger-Pauli JM, Kim W, Guacci V, Onn I, Gygi SP, Koshland DE (2008) A molecular determinant for the establishment of sister chromatid cohesion. *Science* **321:** 566–569

van den Ent F, Leaver M, Bendezu F, Errington J, de Boer P, Lowe J (2006) Dimeric structure of the cell shape protein MreC and its functional implications. *Mol Microbiol* **62:** 1631–1642

Waizenegger I, Hauf S, Meinke A, Peters JM (2000) Two distinct pathways remove mammalian cohesin from chromosome arms in prophase and from centromeres in anaphase. *Cell* **103:** 399–410

Weitzer S, Lehane C, Uhlmann F (2003) A model for ATP hydrolysis-dependent binding of cohesin to DNA. *Curr Biol* **13:** 1930–1940

Yeh E, Haase J, Paliulis LV, Joglekar A, Bond L, Bouck D, Salmon ED, Bloom KS (2008) Pericentric chromatin is organized into an intramolecular loop in mitosis. *Curr Biol* **18:** 81–90

Zhang J, Shi X, Li Y, Kim BJ, Jia J, Huang Z, Yang T, Fu X, Jung SY, Wang Y, Zhang P, Kim ST, Pan X, Qin J (2008) Acetylation of Smc3 by Eco1 is required for S phase sister chromatid cohesion in both human and yeast. *Mol Cell* **31:** 143–151

